RGNZ/MGPB

Hybrid particle swarm optimization and grey wolf optimizer algorithm for Controlled Source Audio-frequency Magnetotellurics (CSAMT) one-dimensional inversion modelling

Rudarsko-geološko-naftni zbornik
(The Mining-Geology-Petroleum Engineering Bulletin)
UDC: 550:8
DOI: 10.17794/rgn.2023.3.6

Original scientific paper

Wahyu Eko Junian[1,3]; Hendra Grandis[1,2]

[1] *Faculty of Mining and Petroleum Engineering, Institut Teknologi Bandung (ITB), Jalan Ganesha 10, Bandung 40132, Indonesia,*

[2] *https://orcid.org/0000-0001-5778-7711*

[3] *Dept. of Geophysical Engineering, Institut Teknologi Sumatera (ITERA), Jalan Terusan Ryacudu, Way Hui, Lampung Selatan 35365, Indonesia*

Abstract

The Controlled Source Audio-frequency Magnetotellurics (CSAMT) is a geophysical method utilizing artificial electromagnetic signal source to estimate subsurface resistivity structures. One-dimensional (1D) inversion modelling of CSAMT data is non-linear and the solution can be estimated by using global optimization algorithms. Particle Swarm Optimization (PSO) and Grey Wolf Optimizer (GWO) are well-known population-based algorithms having relatively simple mathematical formulation and implementation. Hybridization of PSO and GWO algorithms (called hybrid PSO-GWO) can improve the convergence capability to the global solution. This study applied the hybrid PSO-GWO algorithm for 1D CSAMT inversion modelling. Tests were conducted with synthetic CSAMT data associated with 3-layer, 4-layer and 5-layer earth models to determine the performance of the algorithm. The results show that the hybrid PSO-GWO algorithm has a good performance in obtaining the minimum misfit compared to the original PSO and GWO algorithms. The hybrid PSO-GWO algorithm was also applied to invert CSAMT field data for gold mineralization exploration in the Cibaliung area, Banten Province, Indonesia. The algorithm was able to reconstruct the resistivity model very well which is confirmed by the results from inversion of the data using standard 2D MT inversion software. The model also agrees well with the geological information of the study area.

Keywords:

CSAMT; nonlinear inversion; particle swarm optimization; grey wolf optimizer; hybrid algorithm

1. Introduction

Controlled Source Audio-frequency Magnetotellurics (CSAMT) is an electromagnetic (EM) sounding method employing an artificial source to infer the subsurface resistivity distribution. The transmitter (Tx) generates a high-power current injected into the earth through a pair of electrodes forming a horizontal electric dipole along a supposed *x*-axis. At a distance of 5 to 10 km from the source, the receiver (Rx) performs measurement of EM fields variations from pairs of electrodes and coil magnetometers as electric and magnetic field sensors, respectively. The use of an artificial source was proposed in the late 70's to overcome the problem with random and low signals encountered in magnetotellurics (MT) with a natural EM field (**Goldstein and Strangway, 1975**). A typical field configuration for CSAMT is shown in **Figure 1**, where an electric field from dipoles along the *x*-axis (E_x) and a perpendicular magnetic field (H_y) from a coil magnetometer at the center of the array are measured and result in a scalar impedance (Z_{xy}) as CSAMT data. The scalar mode measurement is intended to avoid complicated field logistics, since vector and tensor modes require separate orthogonal sources and measurement of complete horizontal EM field components (**Wannamaker, 1997; Zonge and Hughes, 1991**). CSAMT method is effective in estimating resistivity variations with depth up to 1 to 2 km and sometimes to 3 km depending on the frequency range used, that usually spans from 10 kHz down to 10 Hz or 1 Hz corresponding to periods from 0.0001 sec. to 0.1 sec. or 1 sec. Applications of CSAMT include explorations for geothermal (**Zhao et al., 2019; Zhang et al., 2022**), groundwater petroleum (**Younis et al., 2015; Zhang et al., 2021**) and mineral deposits (**Liu et al., 2020; Zhang et al., 2020**).

Basically, scalar CSAMT data can only be interpreted in terms of a one-dimensional (1D) model, where resistivity varies only with depth. However, with an apparent high lateral resolution due to the separation of only 25 m up to 100 m of the sounding sites along the profile, concatenating 1D models from each station can be used to generate a quasi-2D resistivity model. In MT and CSAMT, 1D inversion modelling is a relatively complex

Corresponding author: Hendra Grandis
e-mail address: grandis@itb.ac.id

problem due to the highly non-linear relationship between data and model parameters, i.e. the resistivity and thickness of the horizontal layers forming the 1D model. Therefore, global optimization methods are often favoured to overcome fundamental problems often encountered in local search or gradient-based inversions, i.e. possible convergence to local minima and sensitivity to the initial model selection (**Wen et al., 2019; Grandis and Sungkono, 2022**). In recent years, population-based global optimization algorithms are gaining interest to resolve complex problems in engineering and extended to geophysical inversions. In such methods, the search space is explored by a population of models serving as search agents. The latter follows perturbation mechanisms often adopted or simulated from natural phenomena (**Yang and He, 2019**). Applications of population-based optimization algorithms for geophysical inversions include particle swarm optimization (PSO) (**Godio and Santilano, 2018; Grandis and Maulana, 2017; Hapsoro et al., 2021; Shaw and Srivastava, 2007; Su et al., 2023**), grey wolf optimizer (GWO) (**Chandra et al., 2017; Li et al., 2018**), artificial bee colony (ABC) algorithm (**Wen et al., 2019**) and symbiotic organisms search (SOS) (**Grandis and Sungkono, 2022; Sungkono and Grandis, 2021**) and many others.

The PSO algorithm was first introduced by **Kennedy and Eberhart (1995)** to solve optimization problems with non-linear functions, by adopting individual and social learning behaviours of a swarm in search for a common target. PSO has been widely used to solve optimization problems in various scientific fields due to its relatively simple implementation with only a few parameters to adjust. Despite modifications to improve its capabilities, various PSO versions still have some weaknesses when applied to complex problems, such as premature convergence, poor exploration capabilities and slow convergence speed (**Cheng et al., 2021; Phung and Ha, 2021**). On the other hand, GWO was first introduced by **Mirjalili et al. (2014)** as an optimization algorithm inspired by the social hierarchy and hunting mechanisms of grey wolves. GWO has simple mathematical formulations with a few tuning parameters and has been applied to solve engineering design problems. The original GWO algorithm also has weaknesses, such as its tendency to stagnate in the exploitation stage and the convergence speed that gradually slows down at the end of the iterations (**Teng et al., 2019**). As an alternative to improvement of each algorithm, combining PSO and GWO called hybrid PSO-GWO algorithm was proposed, especially to improve the convergence (**Singh and Singh, 2017; Cheng et al., 2021**). For example, an original hybrid PSO-GWO has been successfully implemented to solve individual and joint 1D inversion problems for direct current (DC) resistivity and MT data (**Sarkar et al., 2023**).

In this study, the same ratio between the exploration and exploitation stages in the original GWO is modified to become 70:30 by using the exponential decay function to accelerate convergence while maintaining a good exploration capability of the search space. Increasing the percentage of the exploration stage improves GWO ability to search for global information from the objective function (**Mittal et al., 2016**). In the exploitation stage, the solution search is carried out around the first three best solution candidates from GWO by using the PSO concept. This paper describes the application of the hybrid PSO-GWO algorithm for solving a geophysical inverse problem, in particular CSAMT 1D modelling. This study focuses on the implementation of the modified hybrid PSO-GWO optimization algorithm to minimize a relatively complex misfit function involving the CSAMT 1D forward modelling developed by **Fu et al. (2019)**. The latter is optimized such that a large number of forward modelling calculations needed in a global search approach can be done efficiently by using currently available computational resources. The proposed hybrid PSO-GWO algorithm was tested for inversion of synthetic CSAMT data associated with 3-layer, 4-layer and 5-layer earth models with correct and incorrect prior information on the number of layers. Furthermore, the validity of the algorithm was also tested by inversion of real or field data from mineral (gold) exploration in the Cibaliung area, Banten Province, Indonesia leading to satisfactory results.

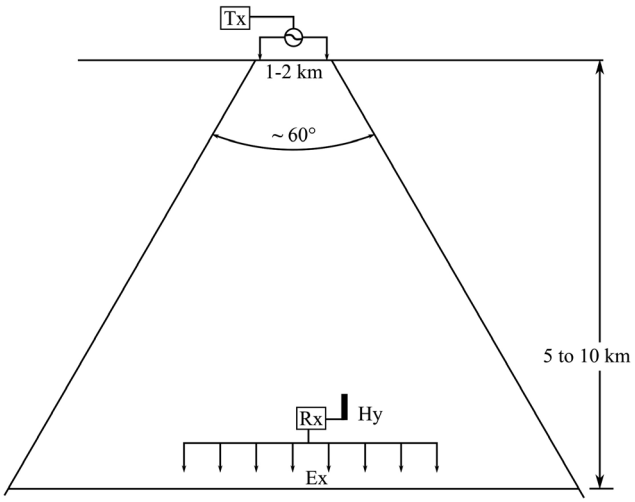

Figure 1: Schematic of a typical field configuration of CSAMT sounding, Tx and Rx are transmitter and receiver, respectively. Ex represents electrodes as electric field sensors and Hy represents coil magnetometer as magnetic field sensor.

2. Hybrid PSO-GWO Algorithm

In what follows, the basic PSO is described according to **Kennedy and Eberhart (1995)** and **Pace et al. (2021)**. In PSO, a population of solution candidates update their positions to search for an optimum area in the search space, by learning individually and socially from their environment. For that purpose, each member of the

population learns from their previous best position (personal best) and from their current movement (inertia) that may bring them to a better position. They also try to move towards the best position achieved by other members (global best). An initial population of size p consisting of models $[\mathbf{x}_k]$; $k = 1,2,\ldots, p$ is generated randomly in the search space. Each model $\mathbf{x}$ is composed by m model parameters, hence $\mathbf{x} = [x_i]$; $i = 1,2,\ldots, m$ is a vector in an m-dimensional search space. At each iteration, the models are updated to sample the search space while converging towards the target, i.e. the minimum misfit between observed and calculated data. The latter is the model response obtained by evaluating the forward modelling function for a particular model. For any k^{th} model current position at t is updated by the velocity at (t+1) as follows (**Pace et al., 2021; Singh and Singh, 2017**),

$$\mathbf{x}_k(t+1) = \mathbf{x}_k(t) + \mathbf{v}_k(t+1) \quad (1)$$

The velocity $\mathbf{v}$ at (t+1) in **Equation 1** is composed by the current velocity and acceleration terms expressed by (**Pace et al., 2021; Sarkar et al., 2023**),

$$\mathbf{v}_k(t+1) = w\mathbf{v}_k(t) + c_1R_1(0,1)\left(\mathbf{p}_k(t) - \mathbf{x}_k(t)\right) + c_2R_2(0,1)\left(\mathbf{g}(t) - \mathbf{x}_k(t)\right) \quad (2)$$

where $\mathbf{p}_k$ represents the personal best, $\mathbf{g}$ is the global best, while c_1 and c_2 are coefficients to control the movement tendency of a model according to individual and social cognitive, respectively. R_1 (0,1) and R_2 (0,1) are random numbers uniformly distributed between 0 and 1 to include stochastic behaviors of the process. The tendency to continue in the current direction is expressed by the current velocity or $\mathbf{v}(t)$ with w as the inertia weight. The latter is commonly set linearly decreasing to the final iteration to limit the perturbation of models as they approach the target. For an iteration equivalent to a unit time step t, velocity and acceleration terms in **Equation 2** can be represented simply by the difference between vector positions in the model space. Hence, the current velocity is calculated in practice as (**Grandis and Maulana, 2017**),

$$\mathbf{v}_k(t) = \mathbf{x}_k(t) - \mathbf{x}_k(t-1) \quad (3)$$

The GWO algorithm as described originally by **Mirjalili et al. (2014)** and later reviewed by **Dada et al. (2022)** was inspired by social hierarchy and hunting mechanisms of a pack of grey wolves in nature. The prey represents the solution being sought, while the wolves are the search agents or solution candidates. The social hierarchy shows the closeness of the search agents to the actual solution. The main stages carried out in GWO consist of tracking, encircling, and attacking prey. The first stage is implemented by identifying alpha, beta, and delta wolves or $\mathbf{x}_\alpha$, $\mathbf{x}_\beta$, $\mathbf{x}_\delta$ which are the first, second and third best solution candidates, respectively. Other solution candidates are $\mathbf{x}_\omega$ or simply $\mathbf{x}$. The encircling prey mechanism is for keeping the prey in the hunting area, while the attacking stage is the movement towards the prey. These can be stated in general form by the following equations (**Mirjalili et al., 2014; Chandra et al., 2017**),

$$\mathbf{D} = \left|\mathbf{C}.\mathbf{x}_{prey}(t) - \mathbf{x}(t)\right| \quad (4)$$

$$\mathbf{x}(t+1) = \mathbf{x}_{prey}(t) - \mathbf{A}\ .\mathbf{D} \quad (5)$$

where all involved vectors have the dimension of $\mathbf{x}$ i.e. the position of a solution candidate, coefficient vectors $\mathbf{A} = 2\boldsymbol{a}.\mathbf{R}_1(0,1) - \boldsymbol{a}$ and $\mathbf{C} = 2\mathbf{R}_2(0,1)$, while $\mathbf{x}_{prey}$ is the position vector of the target, $\boldsymbol{a}$ is a vector whose elements are identical and linearly decaying from 2 to 0 during the iteration process. $\mathbf{R}_1$ (0,1) and $\mathbf{R}_2$ (0,1) are vectors of random numbers uniformly distributed between 0 and 1. The absolute calculation and multiplication of vectors in **Equation 4** and **Equation 5** are operations on an element-by-element basis. Therefore, $\mathbf{D}$ is also a vector in the search space. Similar operations also apply for the subsequent paragraphs.

In reality, the location of the target in the search space is unknown. The solution candidates represented by $\mathbf{x}_\alpha$, $\mathbf{x}_\beta$, $\mathbf{x}_\delta$ have better knowledge of the potential location of the target. Therefore, other solution candidates $\mathbf{x}$ update their positions according to the positions of those three best search agents. The general mechanisms in **Equation 4** and **Equation 5** become (**Mirjalili et al., 2014; Dada et al., 2022**),

$$\mathbf{D}_\alpha = \left|\mathbf{C}\ .\mathbf{x}_\alpha(t) - \mathbf{x}(t)\right|, \mathbf{D}_\beta = \left|\mathbf{C}\ .\mathbf{x}_\beta(t) - \mathbf{x}(t)\right|, \mathbf{D}_\delta = \left|\mathbf{C}\ .\mathbf{x}_\delta(t) - \mathbf{x}(t)\right| \quad (6)$$

$$\mathbf{x}_1 = \mathbf{x}_\alpha - \mathbf{A}_1\cdot\mathbf{D}_\alpha,\ \mathbf{x}_2 = \mathbf{x}_\beta - \mathbf{A}_2\cdot\mathbf{D}_\beta,\ \mathbf{x}_3 = \mathbf{x}_\delta - \mathbf{A}_3\cdot\mathbf{D}_\delta \quad (7)$$

Finally, the position of any solution candidate $\mathbf{x}$ for the next iteration (t + 1) is updated according to the position of the best three solution candidates (α, β and δ), which is expressed by the following equation (**Mirjalili et al., 2014; Chandra et al., 2017; Li et al., 2018**),

$$\mathbf{x}(t+1) = (\mathbf{x}_1 + \mathbf{x}_2 + \mathbf{x}_3)/3 \quad (8)$$

Mathematically, the mechanism of approaching the target is represented by the decay of the value of $\boldsymbol{a}$. However, the resulting coefficient $\mathbf{A}$ will determine the movement of the search agent. It will move closer to the target if $|\mathbf{A}| < 1$ or it turns away from the current target to search for better target. This behaviour allows the GWO algorithm to search for solutions globally.

The hybrid PSO-GWO algorithm combines the advantages of PSO and GWO resulting in better optimization. The mechanism in the hybrid PSO-GWO algorithm is basically an extensive search space exploration through the advantages of the modified GWO algorithm. In this case, the encircling mechanism in **Equation 6** is modified by giving the inertia weight w which is the con-

trol parameter in the PSO algorithm, so that the equation can be written as (**Sarkar et al., 2023; Singh and Singh, 2017**),

$$\mathbf{D}_\alpha = \left|\mathbf{C}\ .\mathbf{x}_\alpha(t) - w\mathbf{x}(t)\right|, \mathbf{D}_\beta = \left|\mathbf{C}\ .\mathbf{x}_\beta(t) - w\mathbf{x}(t)\right|,$$
$$\mathbf{D}_\delta = \left|\mathbf{C}\ .\mathbf{x}_\delta(t) - w\mathbf{x}(t)\right| \quad (9)$$

Then, the candidate solutions from the first three best models are updated by using **Equation 7**. However, instead of using **Equation 8** directly to update a model, the best three candidate solutions obtained from the GWO algorithm (α, β and δ) are used in the PSO mechanism, i.e. to replace personal best and global best, such that the velocity for the next iteration in **Equation 2** is modified to become (**Sarkar et al., 2023; Cheng et al., 2021**),

$$\mathbf{v}_k(t+1) = w\mathbf{v}_k(t) + c_1R_1(0,1)\left(\mathbf{x}_1 - \mathbf{x}_k(t)\right) +$$
$$+ c_2R_2(0,1)\left(\mathbf{x}_2 - \mathbf{x}_k(t)\right) + c_3R_3(0,1)\left(\mathbf{x}_3 - \mathbf{x}_k(t)\right) \quad (10)$$

where c_1, c_2 and c_3 are coefficients to control the movement tendency of a model according to $\mathbf{x}_\alpha$, $\mathbf{x}_\beta$ and $\mathbf{x}_\delta$, respectively. R_1 (0,1), R_2 (0,1) and R_3 (0,1) are random numbers uniformly distributed between 0 and 1.

The inertia weight w in **Equation 9** and **Equation 10** is a control factor in exploration and exploitation during the search process. The exploration stage has a larger inertia weight, and the exploitation stage has a smaller inertia weight. In this study the inertia weight at t is calculated by the following equation (**Sarkar et al., 2023**),

$$w(t) = w_{\max} - (w_{\max} - w_{\min})\left(\frac{t-1}{N_t - 1}\right) \quad (11)$$

where w_{max} and w_{min} are the maximum and minimum inertia weights, respectively, while N_t is the number of iterations. On the other hand, the vector coefficient $\boldsymbol{a}$ is used with an exponential decay function of the number of iterations. Following **Mittal et al. (2016)** for iterations with 70% exploration and 30% exploitation, each element of $\boldsymbol{a}$ is expressed by,

$$a = 2\left(1 - \frac{t^2}{N_t}\right) \quad (12)$$

3. Application to Synthetic CSAMT Data

In this study, the PSO, GWO and hybrid PSO-GWO algorithms were applied to synthetic CSAMT data generated from 1D models that corresponds to 3-layer, 4-layer and 5-layer models (see **Table 1**). The EM response of from a dipole current over an *N*-layered model was obtained by applying the forward modelling algorithm developed by **Fu et al. (2019)**. A dipole length (*dL*) of 1 km with a current strength (*I*) of 10 Amperes and a transmitter-receiver distance (*r*) of 6 km were simulated. The impedance from orthogonal electric and magnetic field, i.e., $Z_{xy} = E_x / H_y$, in the period range of 0.00016 to 0.5 sec. (or frequencies from 6400 down to 2 Hz) were sampled at eight points per decade, resulting in 32 periods. Gaussian noise of 5% was added independently to real and imaginary parts of the impedance. The apparent resistivity and phase data as function of the period (*T*) were calculated by using the well-known Cagniard's formula (**Cagniard, 1953**),

$$\rho_a = \frac{T}{2\pi\mu_0}\left|Z_{xy}\right|^2, \phi = \tan^{-1}\left(\frac{\mathrm{Im}(Z_{xy})}{\mathrm{Re}(Z_{xy})}\right) \quad (13)$$

where $\mu_0 = 4\pi 10^{-7}\,\mathrm{H/m}$ is the permeability of the free space, while Re(.) and Im(.) denote real and imaginary parts of a complex number, respectively.

Table 1: Parameters of synthetic models for 1D CSAMT synthetic data generation

Model	Layer	Parameters	
		Resistivity (Ohm.m)	Thickness (m)
Model 1	1	100	300
	2	10	600
	3	1000	-
Model 2	1	10	300
	2	1000	600
	3	100	-
Model 3	1	10	100
	2	500	300
	3	50	500
	4	1000	-
Model 4	1	500	120
	2	90	200
	3	30	300
	4	60	300
	5	800	-

Tests with a population of 100 models and a total of 500 iterations were carried out to determine the performance of the hybrid PSO-GWO algorithm relative to the original PSO and GWO algorithms. These inversion parameters were considered adequate to obtain good solutions while maintaining a reasonable computational time. The initial population was randomly generated in the search space with boundaries for resistivity ranging from 1 to 2000 Ohm.m and layer thickness from 1 to 1000 meters. The choice for *a priori* model parameter intervals is intended to avoid bias to inversion results since they cover a wide range of values (**Grandis and Maulana, 2017**). In PSO, $c_1 = c_2 = c_3 = 0.5$ were chosen, while inertia weights w_{max} and w_{min} were chosen to be 0.9 and 0.4, respectively. The misfit between the observed and predicted data in each iteration was evaluated using the Root Mean Squared (RMS) errors expressed by (**Grandis and Sungkono, 2022**),

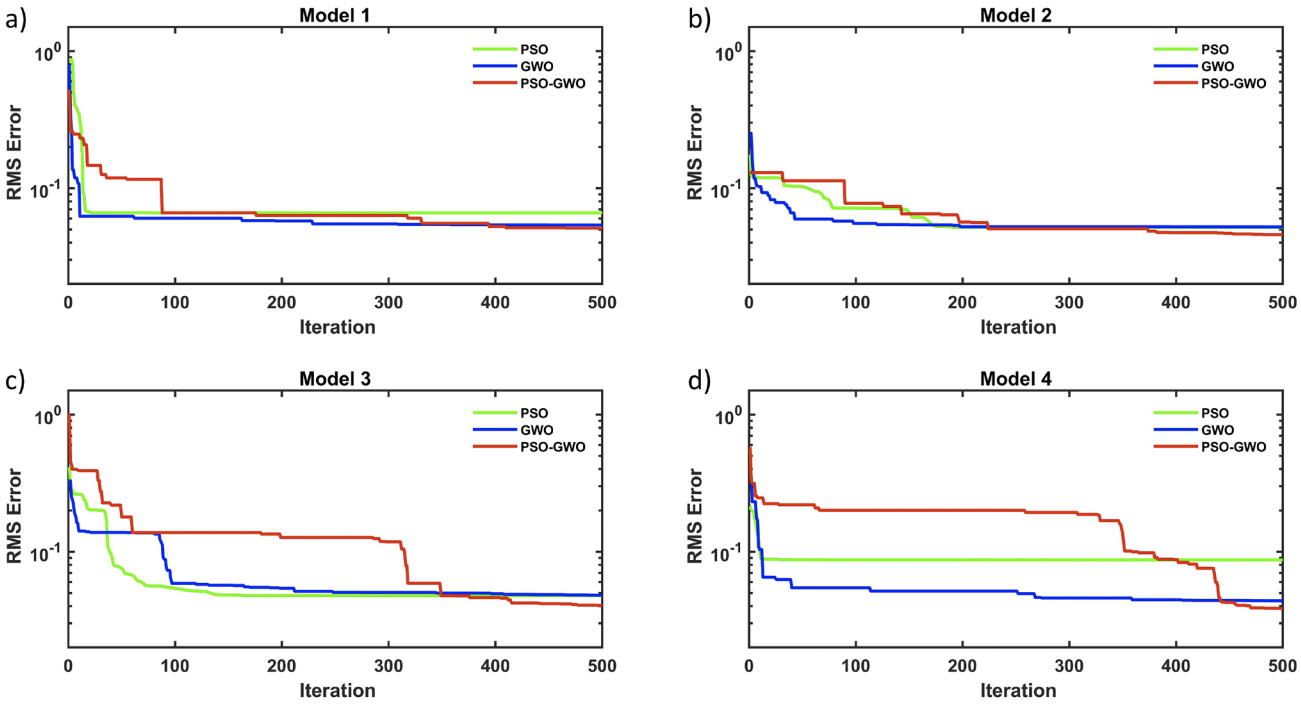

Figure 2: Comparison of misfit as a function of iterations for synthetic data inversion using PSO, GWO and hybrid PSO-GWO algorithms for (a) Model 1, (b) Model 2, (c) Model 3 and (d) Model 4

Table 2: Comparison of the final misfit from synthetic data inversion using the PSO, GWO and hybrid PSO-GWO algorithms

Model	Misfit (RMS Error)		
	PSO	GWO	PSO-GWO
Model 1	0.066	0.054	**0.053**
Model 2	0.052	0.052	**0.049**
Model 3	0.047	0.048	**0.046**
Model 4	0.087	0.044	**0.041**

$$RMS\ Error = \sqrt{\frac{1}{N}\sum_{i=1}^{N}\left(\log\left(\frac{\rho_{a,i}^{obs}}{\rho_{a,i}^{pred}}\right)\right)^2 + \left(\phi_i^{obs} - \phi_i^{pred}\right)^2} \quad (14)$$

Where:

$\rho_{a,i}^{obs}$ and $\rho_{a,i}^{pred}$ are apparent resistivity,

ϕ_i^{obs} and ϕ_i^{pred} are phase for observed and predicted data, respectively,

i is the data index with N is the number of data.

The comparison of the misfit or RMS error versus iterations for inversions with the original PSO, GWO and hybrid PSO-GWO algorithms is presented in **Figure 2** with the best model misfit at the last iteration for all models in **Table 2**. In this case, the hybrid PSO-GWO algorithm converged rather slowly but achieved lower final misfits compared to the original PSO and GWO. Based on the previous similar tests with CSAMT synthetic data, misfit for synthetic data with 5% Gaussian noise relative to data without noise is in the order of 0.05 (**Grandis and Sungkono, 2022**). In these tests, a misfit up to 0.06 is considered acceptable. Such a level of misfit was obtained from almost all algorithms for all models, except for Model 1 and Model 4 with PSO (see **Table 2**). However, **Figure 3** shows qualitatively that there is an overall good fit between synthetic and calculated data (from the best model at the last iteration) presented as sounding curves. The performance of an inversion method is also evaluated by its capability in recovering the synthetic models. **Figure 4** indicates that only hybrid PSO-GWO algorithm can recover the synthetic models remarkably well especially for Model 1 and Model 2, i.e. 3-layer models associated with H-type and K-type sounding curves. The recovery of the synthetic model with a larger number of layers is more difficult, particularly with a 4-layer model with PSO and a 5-layer model with almost all algorithms. Nevertheless, the misfit of the inverse model from the hybrid PSO-GWO for a 5-layer model is exceptionally low. This is due to the equivalence phenomena where slightly different models may result in similar model response that fit to the observed data within an acceptable misfit.

Evaluation of a large number of models in the global optimization algorithm results in relatively more complete information about the objective function in the multi-dimensional space. This allows for the evaluation of the uncertainty of the inverse model. All sampled models from the search space with misfit below 0.06 are plotted in **Figure 5** along with the best model for tests with the hybrid PSO-GWO algorithm. It illustrates qualitatively and visually the inverse model uncertainty for each model tested. A significant variation of model parameter values demonstrates higher uncertainty and dif-

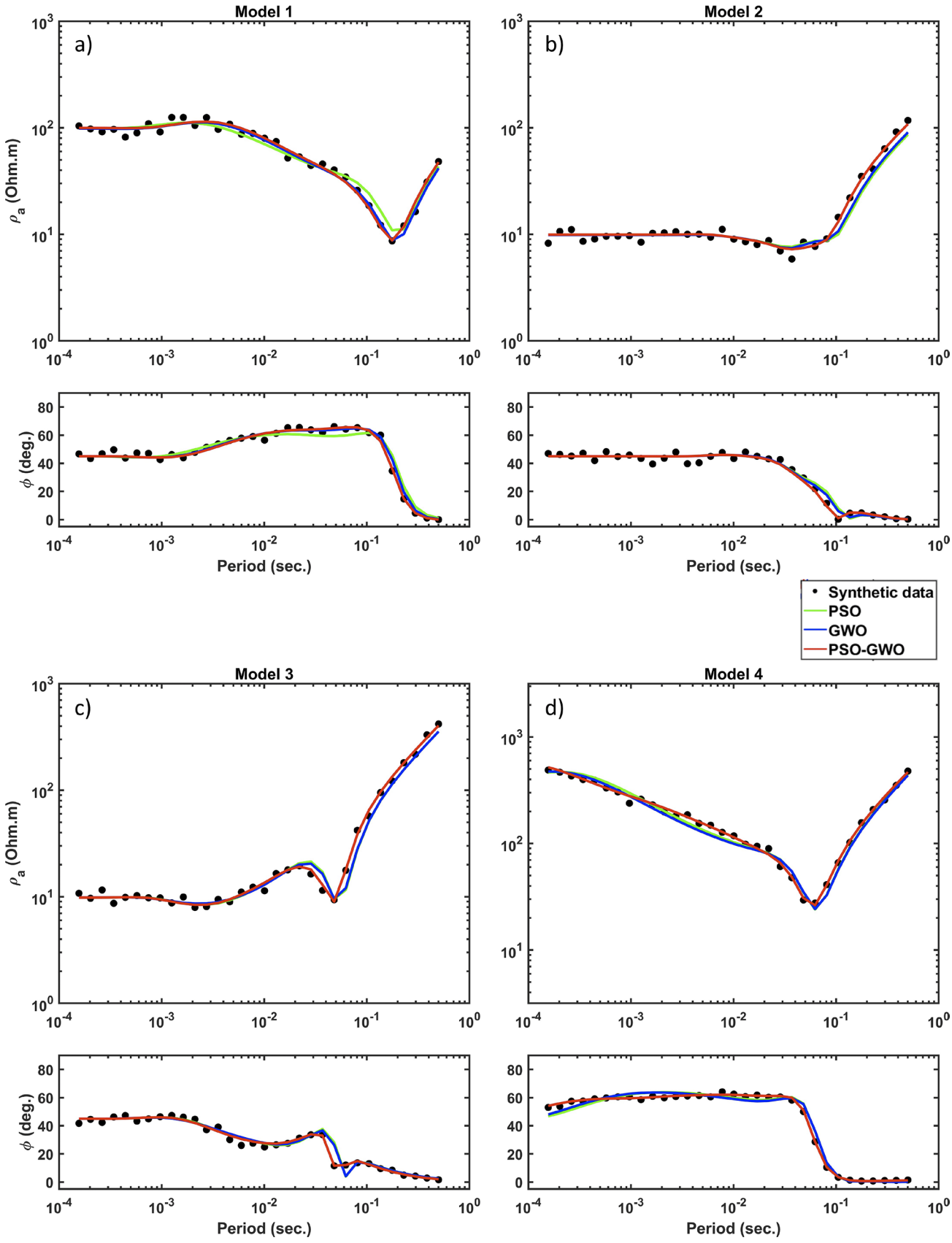

Figure 3: Apparent resistivity (ρ_a) and phase (ϕ) sounding curves of synthetic and predicted data (for the best models at final iteration) from inversion using PSO, GWO and hybrid PSO-GWO algorithms for (a) Model 1, (b) Model 2, (c) Model 3 and (d) Model 4

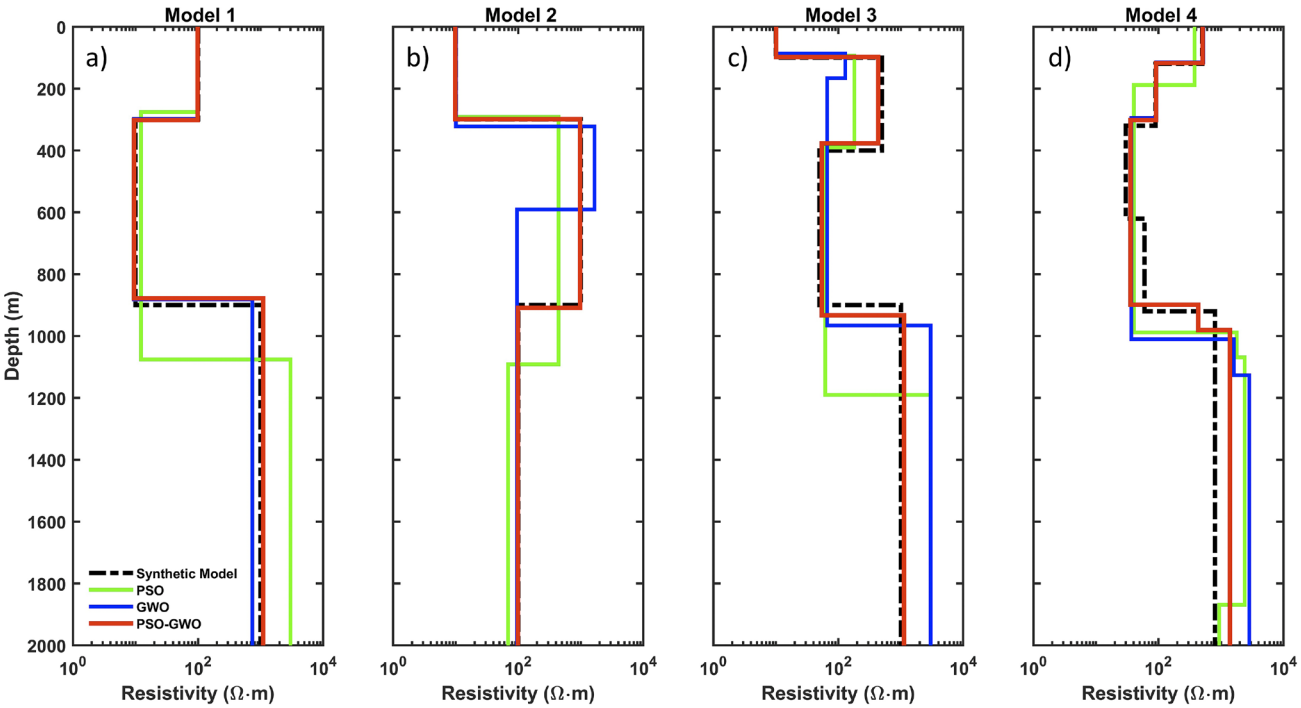

Figure 4: Results from inversion of synthetic data using PSO, GWO and hybrid PSO-GWO compared to the synthetic model for (a) Model 1, (b) Model 2, (c) Model 3 and (d) Model 4. Inverse models are the best model from the last iteration of each algorithm.

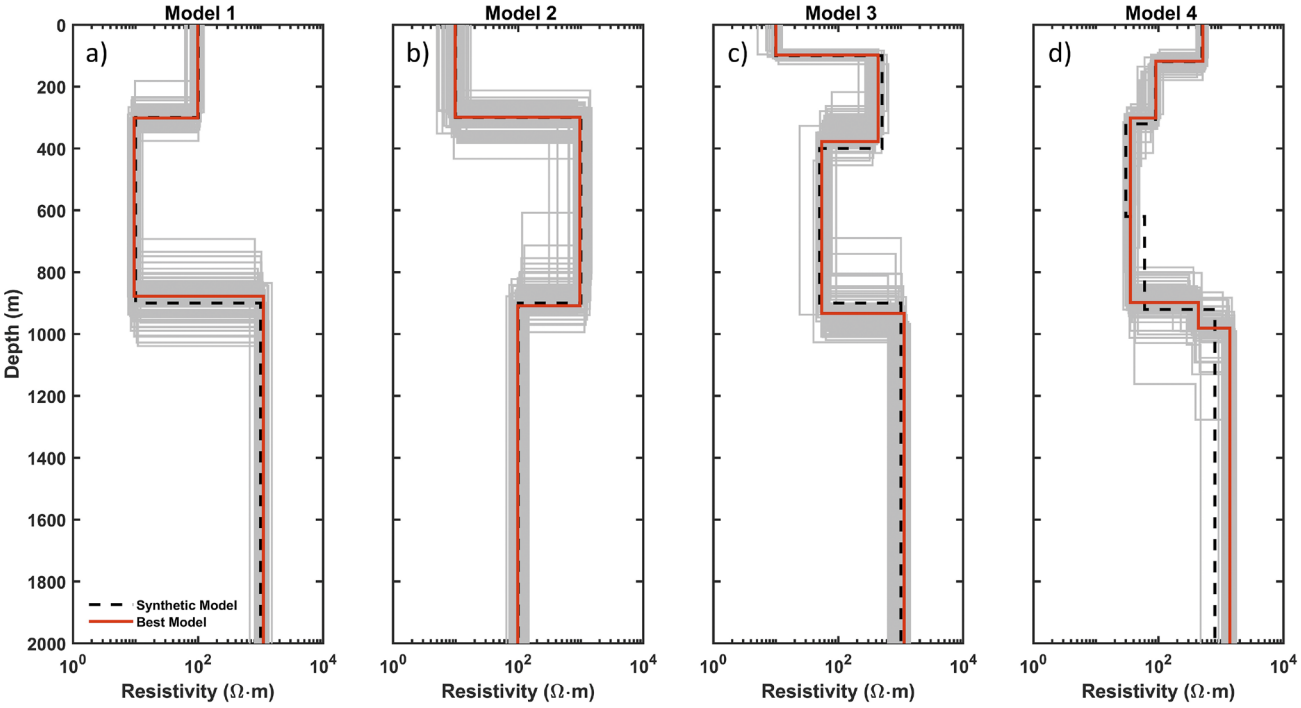

Figure 5: Results from inversion of synthetic data using the hybrid PSO-GWO algorithm for (a) Model 1, (b) Model 2, (c) Model 3 and (d) Model 4. The best models are plotted along with models having misfit below 0.06 (grey lines) and the synthetic models for comparison.

ficulty in resolving a particular model parameter. For example, high uncertainty of thickness of the second layer of Model 1 leads to difficulty in resolving the depth interface of the third or last layer. Quantitatively, the model uncertainty is the standard deviation calculated from each model parameter of the sampled models shown in **Figure 5**. The statistical results of synthetic data inversion using hybrid PSO-GWO algorithm are

Table 3: Model parameters and their uncertainties from synthetic data inversion using the hybrid PSO-GWO algorithm

Model	Layer	Synthetic Model		Inverse Model			RMS Error
		Resistivity (Ohm.m)	Thickness (m)	Resistivity (Ohm.m)	Thickness (m)		
Model 1	1	100	300	98.84 ± 2.5	301.73 ±	8.0	0.053
	2	10	600	9.47 ± 0.3	576.13 ±	15.4	
	3	1000	-	1099.86 ± 30.7	-		
Model 2	1	100	300	9.85 ± 0.2	298.73 ±	7.6	0.049
	2	1000	600	971.12 ± 25.8	607.86 ±	8.2	
	3	10	-	98.22 ± 2.5	-		
Model 3	1	10	100	10.06 ± 0.4	97.64 ±	4.2	0.046
	2	500	300	433.39 ± 26.8	280.13 ±	16.4	
	3	50	500	54.01 ± 3.1	555.66 ±	23.8	
	4	1000	-	1124.22 ± 65.5	-		
Model 4	1	500	120	520.87 ± 24.3	115.30 ±	5.2	0.041
	2	90	200	91.71 ± 4.3	189.29 ±	8.9	
	3	30	300	35.79 ± 1.6	609.63 ±	17.1	
	4	60	300	452.42 ± 23.1	81.89 ±	3.1	
	5	800	-	1465.99 ± 70.6	-		

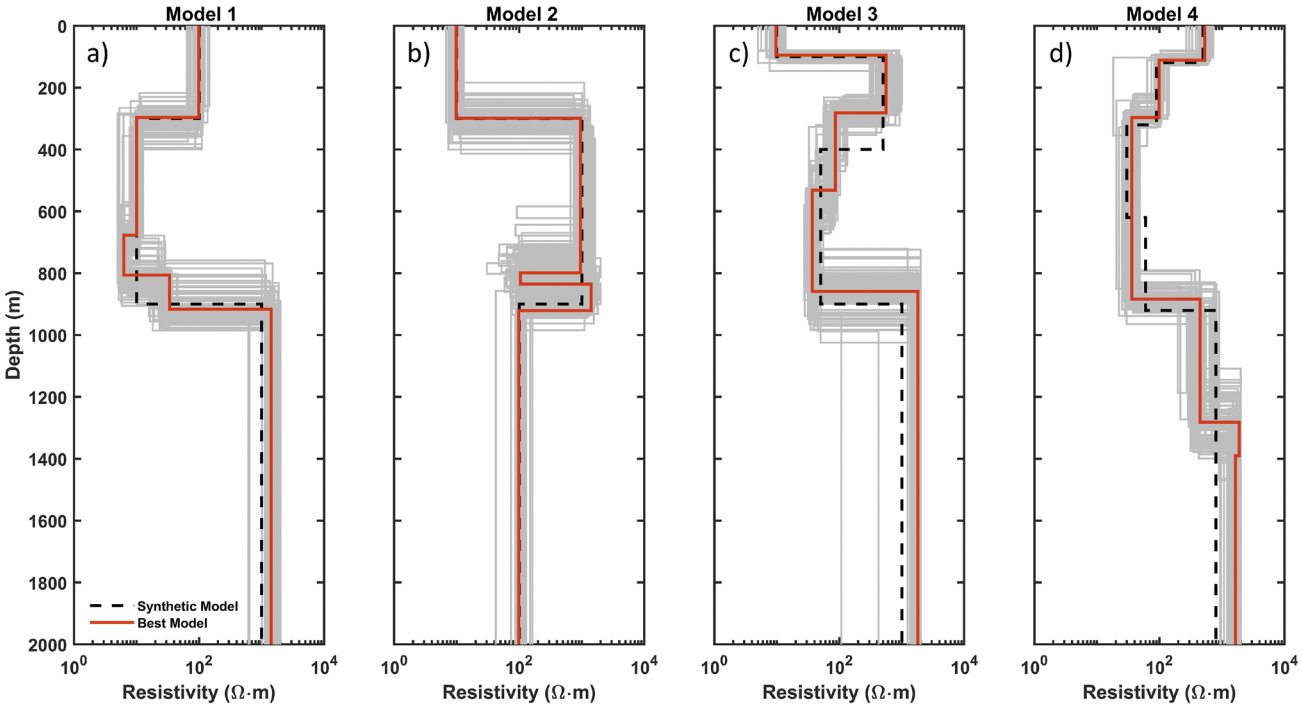

Figure 6: The best models from inversion of synthetic data using the hybrid PSO-GWO algorithm with a different number of layers from the synthetic models, for (a) Model 1 with misfit 0.050, (b) Model 2 with misfit 0.049, (c) Model 3 with misfit 0.047 and (d) Model 4 with misfit 0.045. Models having misfit below 0.06 (grey lines) are plotted along with synthetic models for comparison.

shown in **Table 3**. In general, resistive, and deeper layers are more difficult to resolve. This is in accordance with the basic concept of the general EM sounding method that has good sensitivity for identifying conductive layer and the resolution decreases with increasing depth. The latter is highly related to the diffusive character of the EM fields (**Simpson and Bahr, 2005**).

In reality, the number of layers of the subsurface is unknown in advance. Therefore, all synthetic data were also inverted using the hybrid PSO-GWO algorithm as if they are associated with 5-layer models. In this case, inversions of synthetic data from Model 1, Model 2 and Model 3 were done with an incorrect number of layers. On the other hand, the correct number of layers was used

for the inversion of synthetic data from Model 4. Hence, it was performed only to evaluate the consistency of inversion results for a number of layers most likely encountered in the field. **Figure 6** shows the resulting best model along with all inverse models having misfit below 0.06, including the synthetic models for comparison. Qualitatively, a good resemblance between inverse models with actual synthetic models can be observed. In this case, the uncertainty of the inverse models is not presented quantitatively in terms of standard deviation of model parameters since there is no one-to-one correspondence between the inverse model to the synthetic model with a different number of layers. However, the main feature of resistivity variations with depth can be recovered relatively well by inversion with the hybrid PSO-GWO algorithm. The general characteristics of the EM sounding method are also consistently observed.

4. Application to Field CSAMT Data

Based on the satisfactory performance of the hybrid PSO-GWO algorithm with synthetic data, the algorithm was further tested to invert CSAMT field data associated with mineral exploration in the Cibaliung area, Banten Province, Indonesia. CSAMT soundings were performed along two profiles in the SW-NE direction, approximately perpendicular to the main geological structures of the area at the scale of interest. Line 1 and Line 3 are separated by about 200 m and consist of 57 and 60 sounding sites, respectively. The interval for sounding sites at both profiles is only 25 m, typical of CSAMT survey for mineral resources (see **Figure 7**). The apparent resistivity and phase pseudo-sections of the measured CSAMT data are presented in **Figure 8** and **Figure 9** for Line 1 and Line 3, respectively. Direct interpretation of measured CSAMT data is rarely carried out because the data do not show the true resistivity distribution of the subsurface. However, pseudo-sections indicate qualitatively the resistivity variations, at least laterally along the profile, with cautions for longer period data especially in the near-field zone (**Grandis and Sumintadireja, 2017**). In general, there is no significant difference between those pseudo-sections, implying that the structures are elongated along an assumed direction, i.e. NW-SE or perpendicular to the CSAMT profiles.

All measurement data were inverted using the hybrid PSO-GWO algorithm independently for each CSAMT sounding data. It is assumed that a 4-layer model is adequate to represent the subsurface resistivity variation at every station. Based on the tests with synthetic data, the choice of the number of layers does not have significant effects on the final results. For subsurface represented by a model with less than 4 layers, then the inverse model would show a 4-layer model having layers with similar resistivity or very thin layers with significantly different resistivity. Sample results from inversion of CSAMT field data are presented in **Figure 10** and **Figure 11** for Station 23 of Line 1 and Station 43 of Line 3, respectively. The misfits between the observed and calculated data of the inverse models are in the range of 0.065 to

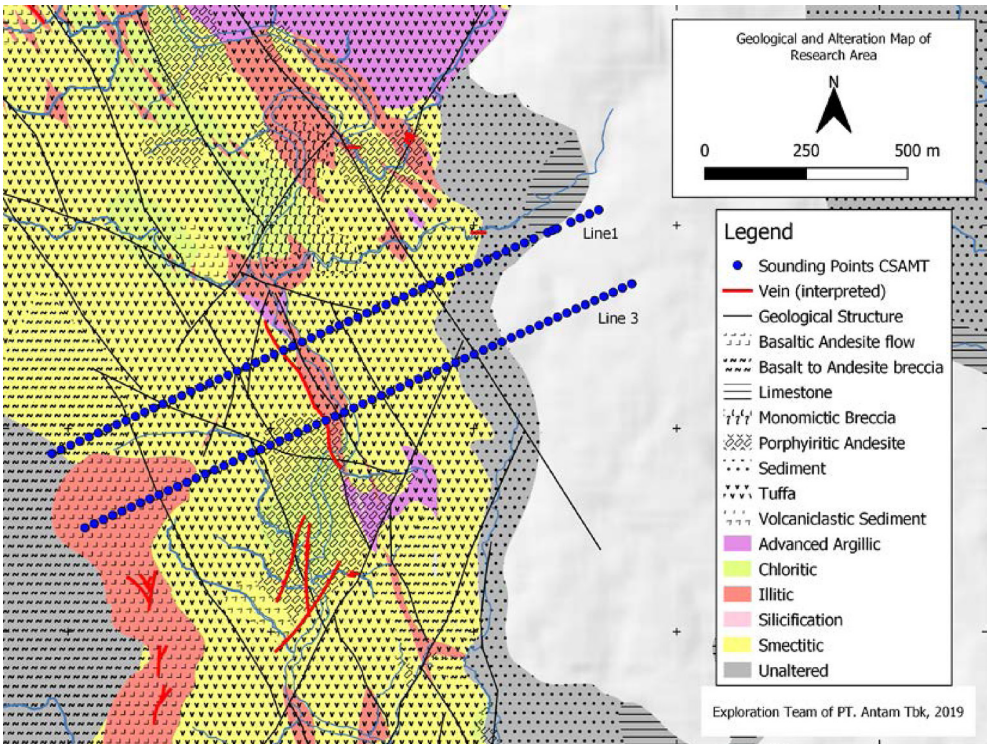

Figure 7: CSAMT sounding locations along Line 1 and Line 3, plotted over the simplified geological and alteration map of the study area.

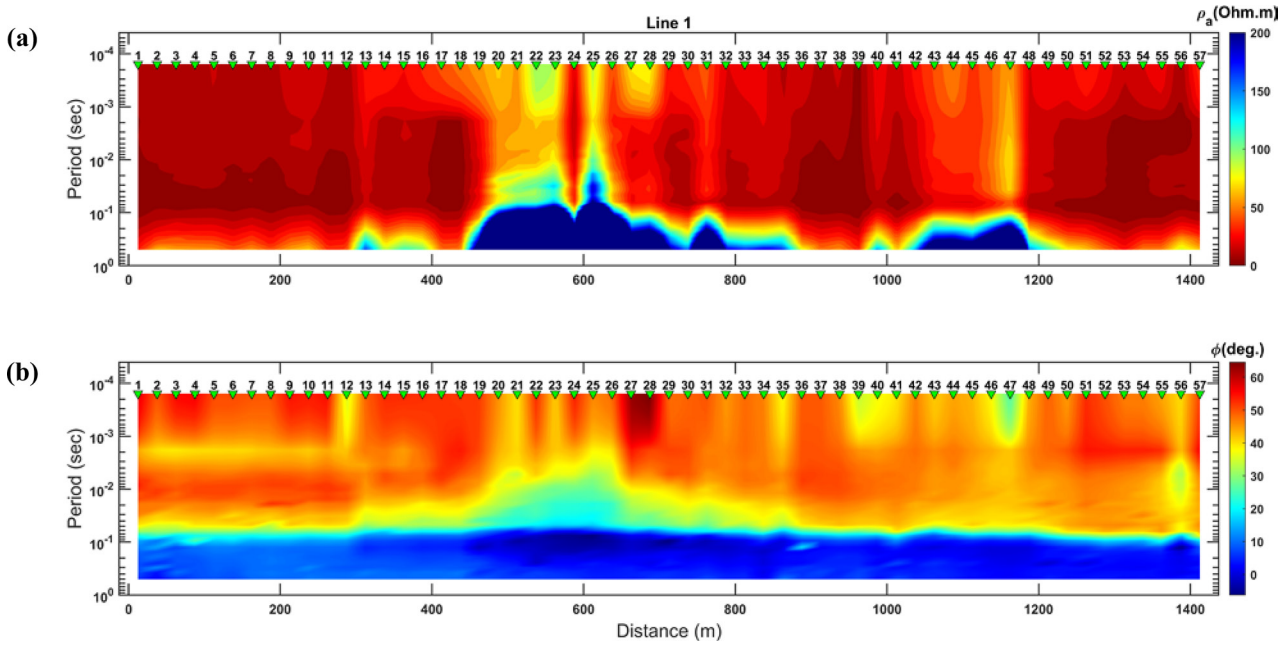

Figure 8: (a) Apparent resistivity and (b) phase pseudo-sections of Line 1. The green inverted triangles with station number indicate the location of sounding points.

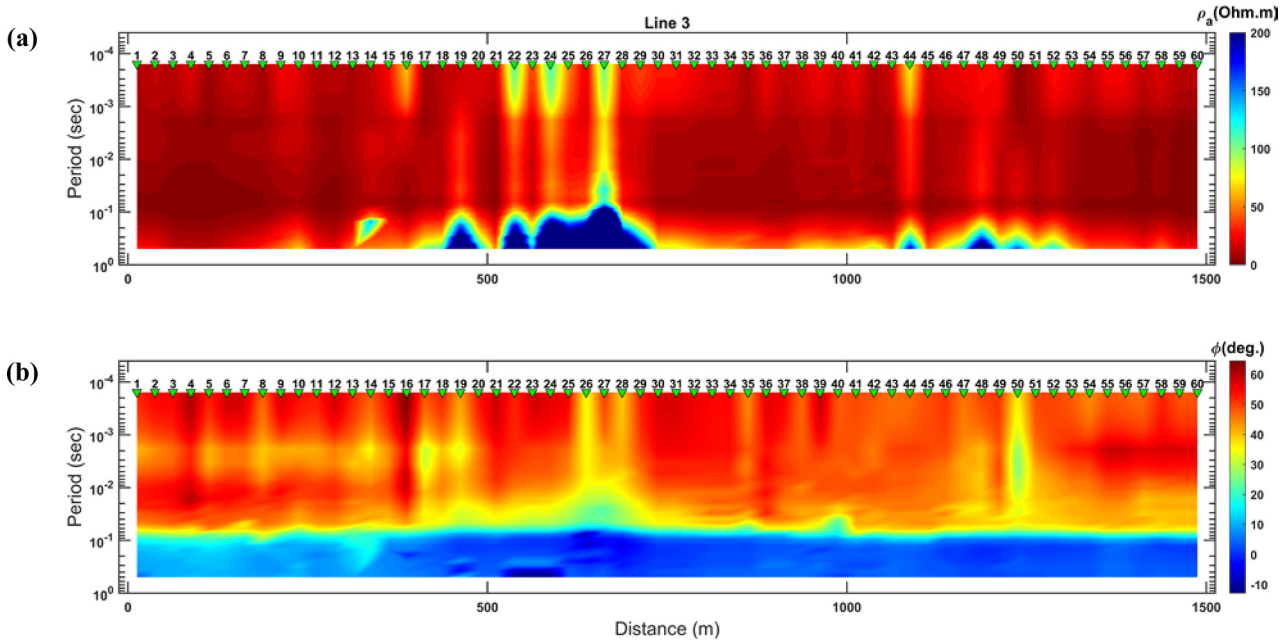

Figure 9: (a) Apparent resistivity and (b) phase pseudo-sections of Line 3. The green inverted triangles with station number indicate the location of sounding points.

0.085 or in general less than 0.1 which is equivalent to an error of approximately 10%.

The inversion modelling results from all sounding stations along each profile are concatenated to obtain a quasi-2D resistivity model and compared to the result of 2D inversion with non-linear conjugate gradient (NLCG) algorithm (**Rodi and Mackie, 2001**) implemented in WinGlink software. In this case, the CSAMT data were limited to cover only the short period range, i.e. to isolate data in far-field condition similar to MT. The latter was done since the software is intended for modelling MT data. In addition, the scalar CSAMT data were considered as TM-mode data only for the structure with strike perpendicular to the profiles. Although both quasi-2D and 2D resistivity models are not quite similar, in general they show a representative subsurface resistivity distribution for the study area (see **Figure 12** and **Figure 13**).

The resistivity model for Line 1 shows a low resistivity layer in the range of 5-100 Ohm.m along the profile

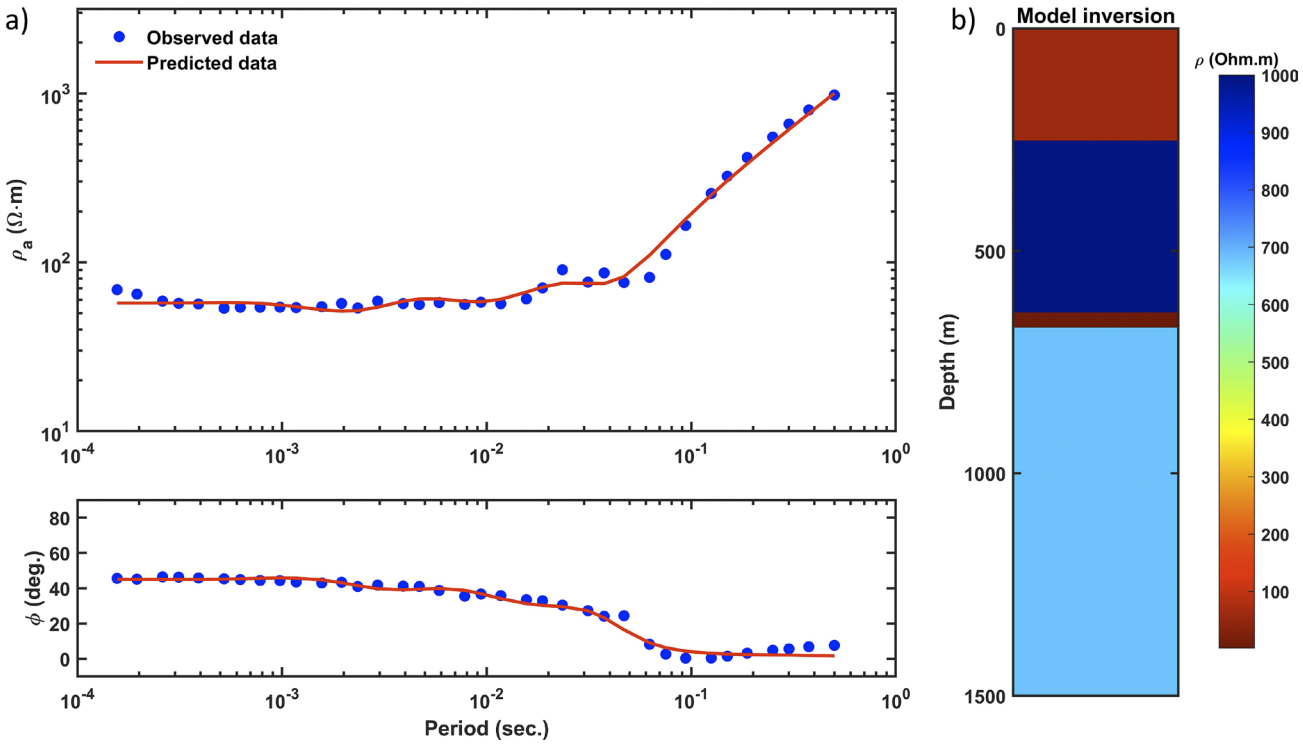

Figure 10: Results from inversion of CSAMT field data at Station 23 of Line 1, (a) apparent resistivity and phase sounding curves showing the fit between observed and calculated data with a misfit of 0.067, (b) 4-layer resistivity model

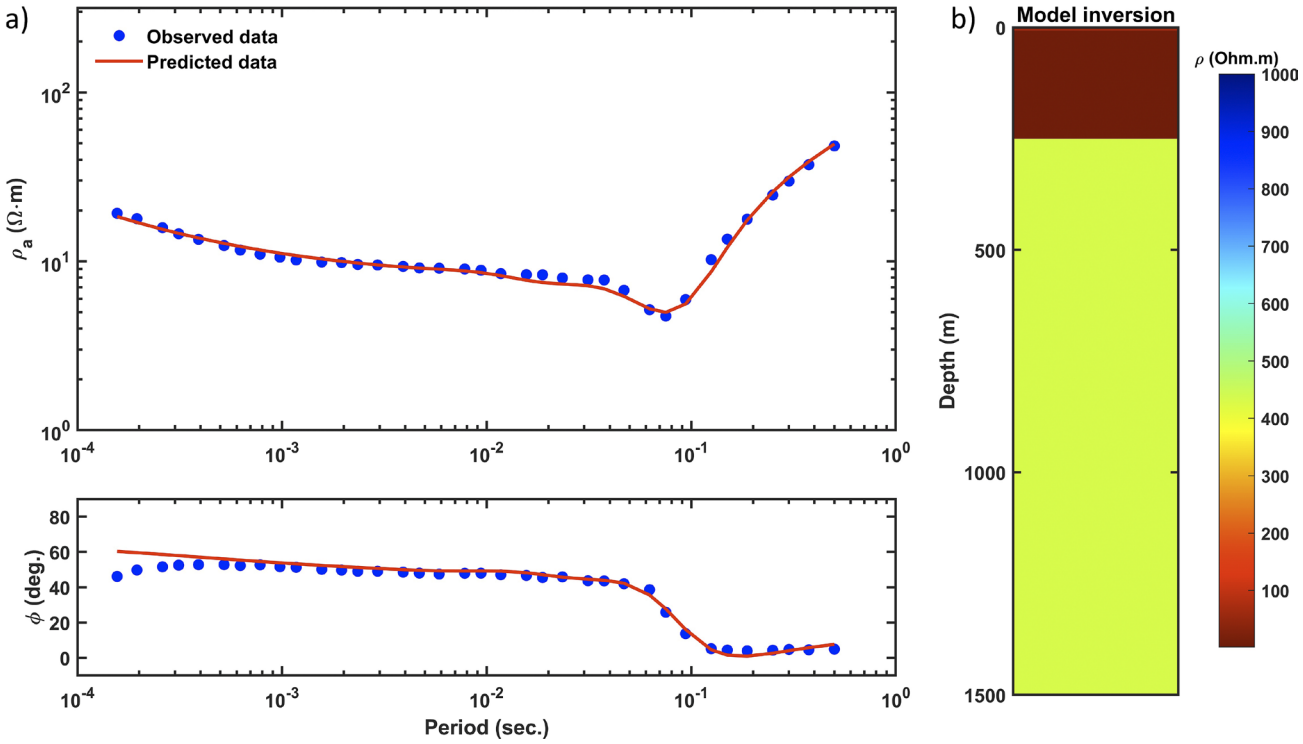

Figure 11: Results from inversion of CSAMT field data at Station 43 of Line 3, (a) apparent resistivity and phase sounding curves showing the fit between observed and calculated data with a misfit of 0.065, (b) 4-layer resistivity model

at shallow depths (from surface down to elevation of -350 m). The superficial low resistivity layer is identified as volcaniclastic sedimentary rocks. There is a contrast between the shallow and deeper zones with a resistivity range of 100-500 Ohm.m. The deeper zone is identified as basement rock composed mostly by pyroclastic breccia. On the other hand, there is a high resistivity anomaly of 500-1000 Ohm.m extending horizontally about 275

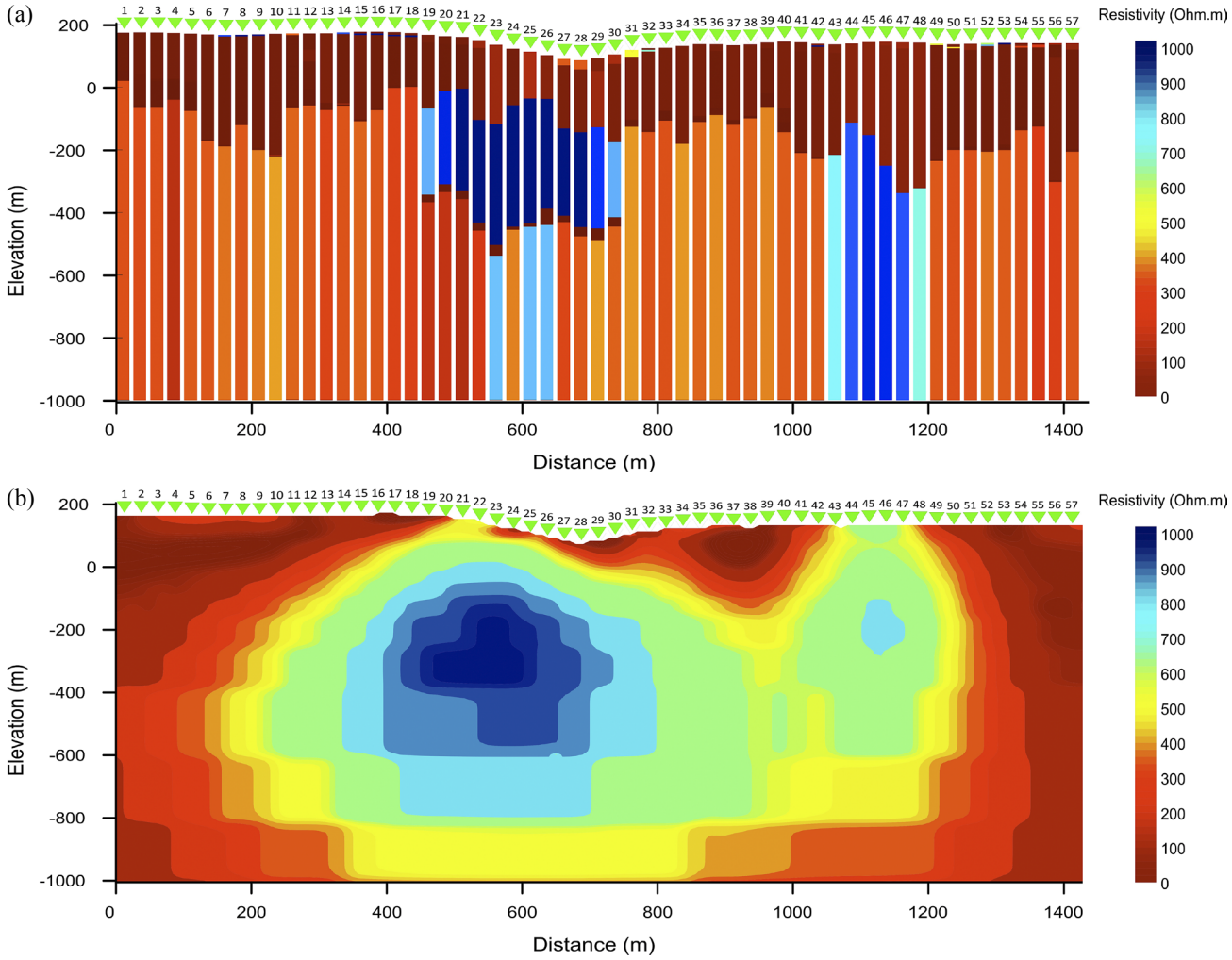

Figure 12: Subsurface resistivity distribution for Line 1 represented by (a) quasi-2D and (b) 2D models (see text for more details)

m from Station 19 to Station 10 at an elevation of -100 to -500 m. This anomaly is thought to be a response to mineralized host rocks (porphyritic andesite) associated with fault structures and clay alteration (illitic and advanced argillic). There is also a high resistivity anomaly with a smaller lateral dimension from Station 43 to Station 48. This anomaly extends vertically to deeper parts of the model and is interpreted as a fault structure and the lithological boundary between altered zone and unaltered zone.

The resistivity model for Line 3 shows a lateral continuation from Line 1 with almost similar character, except that the high resistivity anomaly associated with fault and lithological boundary extends laterally larger, from Station 40 to Station5 1. These results are in accordance with another study using magnetic and induced polarization (IP) methods on the same lines (**Junian et al., 2021a; Junian et al., 2021b**). The area is a mineralization pathway that is controlled by fault structures and illitic alteration (illite-pyrite ± quartz + smectite) with low magnetic anomaly response and high chargeability.

5. Discussion and Conclusions

The particle swarm optimization (PSO) and grey wolf optimizer (GWO) algorithms have proven effective in solving general non-linear optimization problems. However, they are not without drawbacks, such that modifications are still continuously proposed, either by improving characteristic capabilities of individual algorithms or by combining them. In this paper, the hybrid PSO-GWO is presented and implemented for inversion of the 1D inversion modelling of CSAMT synthetic as well as field or real data. The new algorithm has shown a remarkably good performance to solve relatively complex non-linear inversion problems, such as CSAMT 1D modelling by combining the advantages of the original PSO and GWO algorithms. A more extensive search of the model space can be associated with the increase of the ratio between exploration and exploitation to 70:30 as suggested by **Mittal et al. (2016)**, leading to optimum solutions. Inversions of synthetic CSAMT data with 5% Gaussian noise resulted in inverse models with low RMS errors while recovering the synthetic models

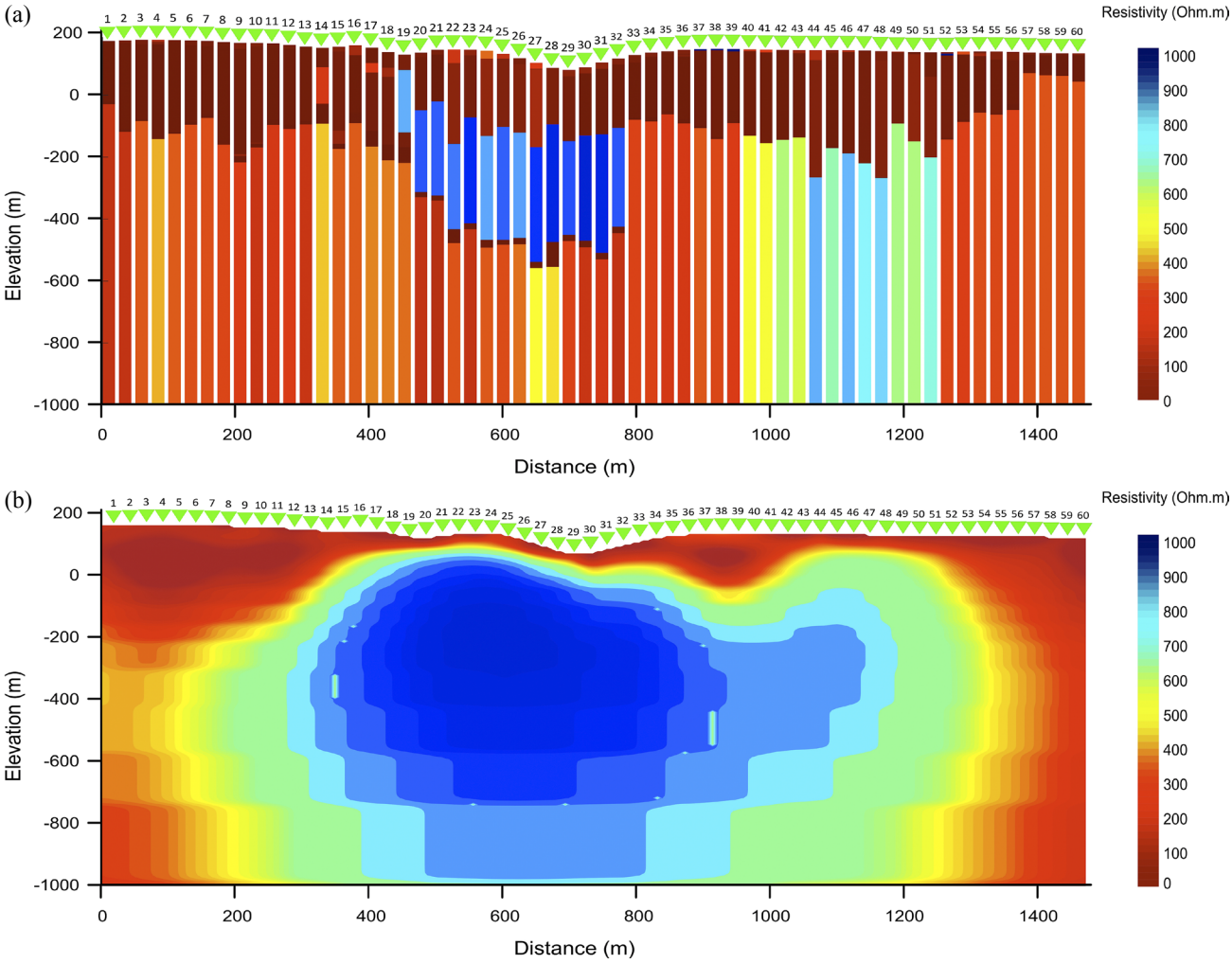

Figure 13: Subsurface resistivity distribution for Line 3 represented by (a) quasi-2D and (b) 2D models (see text for more details)

equally well with the correct or incorrect *a priori* number of layers. Estimation of the number of layers in 1D modelling is more difficult with CSAMT data covering the near-field zone. In the latter, the CSAMT sounding curve contains distortions such that it does not qualitatively represent the resistivity variation with depth (**Grandis and Sumintadireja, 2017**).

In general, the hybrid PSO-GWO algorithm has better performance than the original PSO and GWO algorithms. Its application to invert CSAMT field data results in a subsurface resistivity model showing mineralization zones that are in a good agreement with the local geology of the study area. CSAMT data are mostly obtained with scalar mode measurements and the data reflect simple resistivity variation with depth or 1D. However, concatenating 1D models along a profile to form a quasi-2D model results in a more realistic representation of the subsurface. The latter is supported by the fact that CSAMT sounding stations are closely spaced to each other along a profile, typically only 25 m in mineral prospecting up to 100-200 m in a larger survey coverage, for example in geothermal exploration. By considering only CSAMT data in the far-field zone (high frequencies or short periods) to emulate MT data and use them as TM-mode data, the 2D modelling by using MT 2D inversion software resulted in a 2D model equivalent to quasi-2D model composed of 1D models from the proposed algorithm.

So far, most global population-based optimization algorithms do not have formal mathematical proof of convergence. However, every newly proposed algorithm has undergone tests to find the global minimum of a large number of very complex functions that become standard in the literatures of optimization and its applications. Nevertheless, there are efforts to relate such empirical proof of convergence to more formal or mathematical ones. One of them is the theory of Markov Chain (**Yang and He, 2019**). In this context, more theoretical works are still needed. Furthermore, applications of population-based algorithms are limited to modelling with a small number of model parameters and relatively simple forward modelling. It is mainly determined by the fact that the global optimization approach necessitates misfit evaluation of a large number of models, which is com-

putationally intensive. Hence, extension of the proposed algorithm for vertical electrical sounding (VES), magnetotellurics (MT), transient electromagnetics (TEM) and other similar geophysical methods are rather limited to 1D inversion modelling.

Acknowledgement

The authors would like to thank PT. ANTAM Tbk. for the permission to use the field data in this study. Institute for Research and Community Services ITB is acknowledged for the International Research Grant 2022-2023 to H. Grandis.

6. References

Chandra, A., Agarwal, A., Shalivahan, and Singh, R.K. (2017): Grey wolf optimisation for inversion of layered earth geophysical datasets. Near Surface Geophysics, 15(5), 499-513. https://doi.org/10.3997/1873-0604.2017017

Cagniard, L. (1953): Basic theory of the magneto□telluric method of geophysical prospecting. Geophysics, 18(3), 605-635. https://doi.org/10.1190/1.1437915

Cheng, X., Li, J., Zheng, C., Zhang, J., and Zhao, M. (2021): An improved PSO-GWO algorithm with chaos and adaptive inertial weight for robot path planning. Frontiers in Neurorobotics, 15, 770361. https://doi.org/10.3389/fnbot.2021.770361

Dada, E.G., Joseph, S.B., Oyewola, D.O., Fadele, A.A., Chiroma, H., and Abdulhamid, S.M. (2022): Application of Grey Wolf Optimization algorithm: Recent trends, issues, and possible horizons. Gazi University Journal of Science, 35(2), 485-504. https://doi.org/10.35378/gujs.820885

Fu, H.T., Luo, W.B., Ding, Z.J., Yu, Q.L., and Zhang, S.K. (2019): The calculation on method of whole zone apparent resistivity of vertical magnetic field on the surface of layered model excited by horizontal electrical dipole source. Geophysical and Geochemical Exploration, 43(6), 1309-1319. https://doi.org/10.11720/wtyht.2019.0325

Godio, A., and Santilano, A. (2018): On the optimization of electromagnetic geophysical data: Application of the PSO algorithm. Journal of Applied Geophysics, 148, 163-174. https://doi.org/10.1016/j.jappgeo.2017.11.016

Goldstein, M.A., and Strangway, D.W. (1975): Audio-frequency magnetotellurics with a grounded electric dipole source. Geophysics, 40, 669-683. https://doi.org/10.1190/1.1440558

Grandis, H., and Maulana, Y. (2017): Particle Swarm Optimization (PSO) for magnetotelluric (MT) 1D inversion modeling. *IOP Conference Series: Earth and Environmental Science,* 62, 012033. https://doi.org/10.1088/1755-1315/62/1/012033

Grandis H., and Sumintadireja, P. (2017): Improved pseudo-section representation for CSAMT data in geothermal exploration. *IOP Conference Series: Earth and Environmental Science,* 62, 012035. https://doi.org/10.1088/1755-1315/62/1/012035

Grandis, H., and Sungkono. (2022): Modified symbiotic organisms search (SOS) algorithm for controlled-source audio-frequency magnetotellurics (CSAMT) one-dimensional (1D) modelling. Journal of Earth System Science, 131(1), 61. https://doi.org/10.1007/s12040-021-01808-7

Hapsoro, C.A., Srigutomo, W., Purqon, A., Warsa, W., Sutarno, D., and Kagiyama, T. (2021): Global inversion of grounded electric source time-domain electromagnetic data using particle swarm optimization. Journal of Engineering and Technological Sciences, 53(1), 1-27. https://doi.org/10.5614/j.eng.technol.sci.2021.53.1.1

Junian, W.E., Laesanpura, A., Paembonan, A.Y., and Wicaksono, M.A. (2021a): Identification of gold mineralization zones of low sulfidation epithermal systems using geoelectrical and magnetic methods in Ciparay area, Cibaliung. Journal of Aceh Physics Society, 10(3), 70-79. https://doi.org/10.24815/jacps.v10i3.18521

Junian, W.E., Paembonan, A.Y., Hutami, H.Y., and Wicaksono, M.A. (2021b): Enhanced processing of magnetic data for delineating lithological boundary and geological structure of the epithermal gold mineralization control system - a case study: Cibaliung Area, Indonesia. IOP Conference Series: Earth and Environmental Science, 882, 012047. https://doi.org/10.1088/1755-1315/882/1/012047

Kennedy, J., and Eberhart, R. (1995): Particle swarm optimization. Proceedings of ICNN'95 - International Conference on Neural Networks, 4, 1942-1948. https://doi.org/10.1109/icnn.1995.488968

Kouadio, K.L., Xu, Y., Liu, C.M., and Boukhalfa, Z. (2020): Two-dimensional inversion of CSAMT data and three-dimensional geological mapping for groundwater exploration in Tongkeng Area, Hunan Province, China. Journal of Applied Geophysics, 183, 104204. https://doi.org/10.1016/j.jappgeo.2020.104204

Li, S.Y., Wang, S.M., Wang, P.F., Su, X.L., Zhang, X.S., and Dong, Z.H. (2018): An improved grey wolf optimizer algorithm for the inversion of geoelectrical data. Acta Geophysica, 66, 607-621. https://doi.org/10.1007/s11600-018-0148-8

Liu, G., Meng, X., Tan, H., Chen, Z., Ni, J., and Liu, L. (2020): Case study: Joint seismic reflection and CSAMT data interpretation for mineral explorations in Fujian, China. Acta Geophysica, 68, 1373-1385. https://doi.org/10.1007/s11600-020-00477-2

Mirjalili, S., Mirjalili, S.M., and Lewis, A. (2014): Grey Wolf Optimizer. Advances in Engineering Software, 69, 46-61. https://doi.org/10.1016/j.advengsoft.2013.12.007

Mittal, N., Singh, U., and Sohi, B.S. (2016): Modified Grey Wolf Optimizer for global engineering optimization. https://doi.org/10.1155/2016/7950348

Pace, F., Santilano, A. and Godio, A. (2021): A review of geophysical modeling based on Particle Swarm Optimization. Surveys in Geophysics, 42, 505-549. https://doi.org/10.1007/s10712-021-09638-4

Phung, M.D., and Ha, Q.P. (2021): Safety-enhanced UAV path planning with spherical vector-based particle swarm optimization. Applied Soft Computing, 107, 107376. https://doi.org/10.1016/j.asoc.2021.107376

Rodi, W.L., and Mackie, R. (2001): Nonlinear conjugate gradients algorithm for 2-D magnetotelluric inversion. Geophysics, 66, 174-187. https://doi.org/10.1190/1.1444893

Sarkar, K., Mukesh, M. and Singh, U.K. (2023): Nature-inspired stochastic hybrid technique for joint and individual inversion of DC and MT data. Scientific Reports, 13(1), 2668. https://doi.org/10.1038/s41598-023-29040-x

Shaw, R., and Srivastava, S. (2007): Particle swarm optimization: A new tool to invert geophysical data. Geophysics, 72, F75-F83. https://doi.org/10.1190/1.2432481

Simpson, F., and Bahr, K. (2005): Practical Magnetotellurics. Cambridge University Press.

Singh, N., and Singh, S.B. (2017): Hybrid algorithm of Particle Swarm Optimization and Grey Wolf Optimizer for improving convergence performance. https://doi.org/10.1155/2017/2030489

Su, P., Xu, L., and Yang, J. (2023): 1D regularization inversion combining particle swarm optimization and least squares method. Applied Geophysics (online first). https://doi.org/10.1007/s11770-022-0950-6

Sungkono, S., and Grandis, H. (2021): Improved modified symbiosis organisms search (IMSOS): A new and adaptive approach for determining model parameters from geoelectrical data. Journal of Engineering and Technological Sciences, 53(5), 210505. https://doi.org/10.5614/j.eng.technol.sci.2021.53.5.5

Šumanovac, F., and Orešković, J. (2018): Exploration of buried carbonate aquifers by the inverse and forward modelling of the controlled source audio-magnetotelluric data. Journal of Applied Geophysics, 153, 47-63. https://doi.org/10.1016/j.jappgeo.2018.04.007

Teng, Z.J., Lv, J.L., and Guo, L.W. (2019): An improved hybrid grey wolf optimization algorithm. Soft Computing, 23, 6617-6631. https://doi.org/10.1007/s00500-018-3310-y

Wannamaker, P.E. (1997): Tensor CSAMT survey over the Sulphur Springs Thermal Area, Valles Caldera, New Mexico, USA, Part I: Implications for structure of the Western Caldera. Geophysics, 62, pp. 451-465. https://doi.org/10.1190/1.1444156

Wen, L., Cheng, J., Li, F., Zhao, J., Shi, Z., and Zhang, H. (2019): Global optimization of controlled source audio-frequency magnetotelluric data with an improved artificial bee colony algorithm. Journal of Applied Geophysics, 170, 103845. https://doi.org/10.1016/j.jappgeo.2019.103845

Yang, X.-S., and He, X.-S. (2019): Mathematical Foundations of Nature-Inspired Algorithms. Springer. https://doi.org/10.1007/978-3-030-16936-7

Younis, A., El-Qady, G., Abd Alla, M., Abdel Zaher, M., Khalil, A., Al Ibiary, M., and Saraev, A. (2015): AMT and CSAMT methods for hydrocarbon exploration at Nile Delta, Egypt. Arabian Journal of Geosciences, 8(4), 1965-1975. https://doi.org/10.1007/s12517-014-1354-6

Zhang, C., Yuan, B., Li, Y., Zhang, Q., and Han, L. (2021): Features of apparent resistivity anomaly of controlled-source audio-frequency magnetotellurics and prospects of oil shale in the Tongchuan area of the southern Ordos Basin, China. Interpretation, 9(4), T1055-T1063. https://doi.org/10.1190/int-2020-0083.1

Zhang, J., Zeng, Z., Zhao, X., Li, J., Zhou, Y., and Gong, M. (2020): Deep mineral exploration of the Jinchuan Cu-Ni sulfide deposit based on aeromagnetic, gravity, and CSAMT methods. Minerals, 10, 168. https://doi.org/10.3390/min10020168

Zhang, K., Lin, N., Wan, X., Yang, J., Wang, X., and Tian, G. (2022): An approach for predicting geothermal reservoirs distribution using wavelet transform and self-organizing neural network: A case study of radon and CSAMT data from Northern Jinan, China. Geomechanics and Geophysics for Geo-Energy and Geo-Resources, 8(5), 156. https://doi.org/10.1007/s40948-022-00468-1

Zhao, W., Lin, Y., Zhou, P., and Wang, G. (2019): Systematic analysis of geothermal resources in the coastal bedrock area of Chunxiao Town (China) by using geochemistry and geophysics methods. Water, 11, 214. https://doi.org/10.3390/w11020214

Zhdanov, M.S. (2018): Foundations of Geophysical Electromagnetic Theory and Methods (Second ed). Elsevier. https://doi.org/10.1016/C2014-0-02307-6

Zonge, K.L., and Hughes, L.J. (1991): Controlled Source Audio-Frequency Magnetotellurics. In Electromagnetic Methods in Applied Geophysics. Nabighian, M. (Ed). Society of Exploration Geophysicists (SEG). https://doi.org/10.1190/1.9781560802686.ch9

SAŽETAK

Hibridni algoritam optimizacije roja čestica i optimizacije sivoga vuka za jednodimenzionalno inverzno modeliranje audiofrekvencijske magnetotelurike s kontroliranim izvorom (CSAMT)

Audiofrekvencijska magnetotelurika s kontroliranim izvorom (CSAMT) geofizička je metoda koja se koristi izvorom umjetnoga elektromagnetskog signala za procjenu struktura otpornosti ispod površine. Jednodimenzionalno (1D) inverzno modeliranje CSAMT podataka nelinearno je te se rješenje može procijeniti korištenjem algoritama za globalnu optimizaciju. Algoritam roja čestica (PSO) i algoritam sivoga vuka (GWO) dobro su poznati algoritmi koji se temelje na populaciji i imaju relativno jednostavnu matematičku formulaciju i implementaciju. Hibridizacija PSO i GWO algoritama (hibridni PSO-GWO) može poboljšati sposobnost konvergencije prema globalnom rješenju. U ovom istraživanju primijenjen je hibridni PSO-GWO algoritam za 1D CSAMT inverzno modeliranje. Provedeno je testiranje sa sintetičkim CSAMT podatcima povezanim s 3-slojnim, 4-slojnim i 5-slojnim modelima zemlje kako bi se odredile performanse algoritma. Rezultati su pokazali kako hibridni PSO-GWO algoritam ima dobre performanse u postizanju minimalne neusklađenosti u usporedbi s originalnim PSO i GWO algoritmima. Hibridni PSO-GWO algoritam također je primijenjen za inverziju CSAMT terenskih podataka s ciljem istraživanja mineralizacije zlata u području Cibaliung, provincija Banten, Indonezija. Algoritam je uspio vrlo dobro rekonstruirati model otpornosti, što potvrđuju rezultati inverznoga modeliranja korištenjem standardnoga softvera za inverziju 2D magnetotelurskih podataka. Rezultati modela također se dobro podudaraju s geološkim informacijama istraživanoga područja.

Ključne riječi:
CSAMT, nelinearna inverzija, algoritam roja čestica, algoritam sivoga vuka, hibridni algoritam

Author's contribution

Wahyu Eko Junian (Master's student of Geophysical Engineering Dept. at ITB and Research Assistant at ITERA) conceived the main idea, implemented the algorithm and Matlab script, designed experiments and tests, and wrote the first draft of the manuscript. **Hendra Grandis** (Professor of geophysics at ITB) validated the experimental results and thoroughly reviewed and rewrote the manuscript.